Topics in Catalysis Vol. 44, Nos. 1–2, June 2007 (© 2007)
DOI: 10.1007/s11244-007-0288-6

Factors in gold nanocatalysis: oxidation of CO in the non-scalable size regime

Uzi Landman[a,*], Bokwon Yoon[a], Chun Zhang[a], Ueli Heiz[b], and Matthias Arenz[b]

[a]*School of Physics, Georgia Institute of Technology, Atlanta, GA, 30332-0430 USA*
[b]*Lehrstuhl für Physikalische Chemie I, Technische Universität München, Lichtenbergstrasse 4, 85747 Garching, Germany*

Focusing on size-selected gold clusters consisting of up to 20 atoms, that is, in the size regime where properties cannot be obtained from those of the bulk material through scaling considerations, we discuss the current state of understanding pertaining to various factors that control the reactivity and catalytic activity of such nanostructures, using the CO oxidation reaction catalyzed by the gold nanoclusters adsorbed on MgO as a paradigm. These factors include the role of the metal-oxide support and its defects, the charge state of the cluster, structural fluxionality of the clusters, electronic size effects, the effect of an underlying metal support on the dimensionality, charging and chemical reactivity of gold nanoclusters adsorbed on the metal-supported metal-oxide, and the promotional effect of water. We show that through joined experimental and first-principles quantum mechanical calculations and simulations, a detailed picture of the reaction mechanism emerges.

KEY WORDS: dimethylamine; pyridine; XPS; STM; amide; surface; Cu(110), amine oxide; nanocatalysis; CO oxidation; size selected gold clusters; non-scalable size regime; first principle calculations; active sites; defects; metal oxide films; structural dynamic fluxionality; reaction mechanisms; activation barriers; humidity effects; tuning catalytic activity.

1. Introduction

Characterization and elucidation of the size-dependent evolution of the physical and chemical properties of finite materials aggregates, having discrete quantized energy level spectra, specific structural and morphological motifs and exhibiting unique dynamical characteristics, are among the outstanding challenges of modern materials science. Indeed, investigations of the unique properties of finite materials aggregates, and studies aiming at gaining deep insights into the development of materials characteristics from the molecular and cluster regimes to the bulk phase, are major themes of current interdisciplinary basic and applied research endeavors. In many instances, it is found that for larger materials aggregates the deviations of the properties from the bulk limit scales with the size of the aggregate. However, in many cases, at sufficiently small sizes, which most often lie in the nanoscale regime, the dependence of the material's property on size becomes *non-scalable*, and then *small becomes different* in an essential way, where the physical and chemical properties become emergent in nature, that is, they can no longer be deduced or extrapolated from those known for larger sizes [1].

Nanocatalysis is one of the most exciting subfields of nanoscience. Unlike the common practice in catalysis where the catalytic performance scales with the surface to volume ratio of the dispersed catalytic agent, nanocatalysts are distinguished by their unique and non-scalable properties that originate from the highly reduced dimensions of the active catalytic aggregates. Consequently, the central aim of nanocatalysis is the promotion, enhancement, steering and control of chemical reactions by changing the size, dimensionality, chemical composition, morphology, or charge state of the catalyst or the reaction center, and/or by changing the kinetics through nanopatterning of the catalytic reaction centers. Since the aforementioned size-dependent non-scalable, and often non-monotonic, evolution of materials' properties may occur when at least one of the material's dimensions is reduced to the nanoscale, nanocatalytic systems may appear as ultra-thin films, nanowires or clusters. For these systems the chemical and physical properties are often controlled by quantum size effects and they present new opportunities for an atom-by-atom design, tuning and control of chemical activity, specificity, and selectivity [2].

With the focus of this article being on gold nanocatalysts, we recall first the common experience that in bulk form gold is the noblest of all metals [3–5]. Consequently it has not been considered till quite recently as a possible catalyst. The chemical inertness of gold is reflected in the low adsorption energy of gases participating in a number of catalytic reactions of interest and the lack of activation, and/or high dissociation barriers, of the weakly adsorbed molecules [3]. Additionally, the low melting point of gold hampers the preparation of nanoparticles smaller than 10 nm in diameter [6], which is of importance for maximizing the active surface area of a catalyst.

First results which indicated that small gold particles may act as catalysts were reported in the early 1970s [7,8]. Subsequent work [6,9,10] highlighted the exciting

*To whom correspondence should be addressed.
E-mail: Uzi.landman@physics.gatech.edu

catalytic properties of gold nanoparticles and described methods for the preparation of approximately hemispherical gold particles on selected metal oxides. These studies have shown that gold nanoparticles may exhibit high catalytic activity for various reactions, including CO oxidation and propylene epoxidation. Moreover, it has been demonstrated that Au nanoparticles catalyze some reactions already at rather low temperatures [9] (with CO oxidation reported at temperatures as low as 200 K), thus making them interesting for a series of room temperature applications; for comprehensive lists of applications of gold nanocatalysts see refs. [4,9–15].

Understanding the emergent chemical activity of nanoscale gold particles poses a particularly complex challenge in light of the aforementioned inert nature of this metal in the bulk form. It is therefore not surprising that certain attempts to explain some of the more recent observation about Au nanocatalysis through the use of methodologies developed in the course of investigations of the catalytic activity of other noble metals (e.g. Pt), did not lead to conclusive results and/or were not supported by further experiments. Thus for example in early papers a Langmuir-Hinshelwood mechanism was assumed for the Au-catalyzed CO oxidation reaction, involving the dissociation of oxygen molecules on the Au catalyst [16], as is the case for platinum group metals. The catalytic activity of gold nanoparticles was thus explained by an increased heat of adsorption of oxygen atoms, produced by a hot filament on gold nanoparticles, compared to bulk gold [16,17]. However, it has been discovered through first-principles calculations [18–20] (see below) that independent of the substrate, oxygen adsorbs molecularly (without formation of a dissociated intermediate state) on Au nanoclusters supported on metal oxide, forming activated partially charged species (superoxo- or peroxo-like species) which react with CO to form CO_2 [18–20]. This prediction has been subsequently supported by experiments showing that on reactive Au particles after adsorbing oxygen and pumping of the oxygen in the chamber, no adsorbed oxygen can be anymore titrated by CO pulses, thus demonstrating the absence of dissociative adsorption of oxygen [21]. In fact, it seems that the relatively weak adsorption energy of oxygen on gold and the formation of ''activated'' oxygen molecules, are among the key features underlying the low temperature nanocatalytic activity of gold.

While significant progress has been achieved in the past several years toward fundamental understanding of the materials and operational factors that govern the catalytic activity of gold nanostructures, much remains to be learned. This subject is complicated by the convergence of a number of interdependent factors that can influence and vary the reactivity and reaction pathways, including the identity and nature of the support surface, the preparation procedures used and the ambient conditions (e.g. humidity). In their review, Bond and Thompson [15] summarized as *consensual* observations that: (i) oxide-supported small gold particles show highest reactivity at sizes of about 2–3 nm, whereas unsupported gold particles are weakly active at best; and (ii) the choice of support, the method of preparation and the pretreatment before use, are very important factors controlling the reactivity. These authors also discussed a possible mechanism involving reaction at the edge of a particle involving the support, thus emphasizing the importance of the perimeter interface. Haruta concluded, along similar lines, that the performance of Au nanoparticles is defined by three major factors, the contact structure to the oxide support, the nature of the support and the particle size, with the contact structure being the most important factor [6]. The proposed perimeter model implies direct involvement of the support in the CO oxidation reaction [22]. Furthermore, an enhancement of the catalytic activity of small gold particles due to moisture was reported [23,24]. This is particularly relevant for applications at ambient conditions, since commonly the presence of moisture is found to be detrimental or non-beneficial to their activity. In contrast to the above perimeter model Goodman *et al.* concluded on the basis of investigations involving a bilayer gold model catalyst supported on titania that the role of the TiO_x support is mainly that of a dispersant and a promoter [14,25]. As we discuss below the special role of the adsorbed peripheral interface between the gold nanostructure and the supporting metal-oxide emerges also from recent theoretical studies. Furthermore, it has been suggested that the adsorption propensity of O_2 to finite size Au particles is increased, particularly at low-coordinated sites [18–20,26–30]. The importance of low-coordinated sites is in line with experimental work on supported gold model catalysts that emphasized the influence of highly uncoordinated gold atoms on the CO adsorption properties [31–33].

It is evident from the above brief remarks that the juxtaposition of different preparation procedures, various pretreatment conditions and supports, often poorly characterized catalytic particles (e.g., essentially unknown size, morphology and/or structure), and the strong influence of these factors on the reaction outcome, are not conducive to the development of a comprehensive picture of the interaction processes and reaction mechanisms that underlie gold nanocatalysis. Aiming at disentangling the factors controlling the reactivity of gold and wishing to gain insights into the microscopic origins of the size-dependent reactivity of gold in the nanoscale regime, we believe that further progress can be achieved through investigations of well-defined model systems. Consequently in this brief review, we summarize our experimental and first-principles theoretical endeavors focusing on the CO oxidation reaction catalyzed by *size-selected* gold particles supported on thin metal-oxide films. The size of the

particles which we explore is up to 1 nm in diameter, that is, the size regime in which the electronic, and thus catalytic, properties of the particles cannot be deduced from the bulk behavior through scaling considerations.

2. The size-dependent reactivity of supported Au_n clusters

Au_n clusters were produced by a laser vaporization source [34,35], size-selected in a quadrupole mass spectrometer and deposited with low kinetic energy (<0.2 eV/atom, i.e. softlanding) on thin oxide films [36,37]. A concern that arises when using free clusters to prepare monodispersed cluster materials is the fate of the deposited cluster during and after deposition. In addition to molecular dynamics simulations [38–41], several experiments, such as STM investigations [42,43], or absorption spectroscopy of clusters embedded in a rare gas matrix have been performed, which demonstrate that soft landing of clusters is possible [44]. Also, the studies of the chemical reactivity of supported clusters using pulsed molecular beams show evidence of stability of the samples [45]. Recently, we were able to provide strong evidence in support of the monodispersity of the deposited clusters by using cavity ringdown spectroscopy [46]. In these experiments each gold cluster with up to 20 atoms shows a distinct optical response in the visible photon energy range. In addition, by comparing the optical response of SiO_2-supported Au_1 and Au_2 (figure 1) only an extremely weak atomic feature in the Au_2-spectrum is observed, indicating that post-deposition fragmentation is less than 5%. Furthermore, the spectrum of Au_1 does not reveal any feature of the dimer or larger clusters, indicating that aggregation can be excluded.

Supported, small gold clusters have mainly been deposited on thin MgO(100) films. These thin films can be prepared either as defect-rich films, characterized by a given density (~5% ML) of extended defects and point defects (F-centers), or as defect-poor films with a negligible density of F-centers [18,47]. The oxidation reaction of CO was studied by a combination of temperature programmed reaction (TPR) and Fourier-transform infrared (FTIR) spectroscopy. In these experiments, isotopically labeled $^{18}O_2$ and ^{13}CO molecules were used and the catalytic oxidation of CO involving oxygen atoms from the MgO substrate could be excluded, since only the $^{13}C^{16}O^{18}O$ isotopomer was detected. Both defect-poor as well as defect-rich bare MgO films, are inert for CO oxidation [18].

As illustrated in figure 2, gold clusters with up to seven atoms are inert for CO oxidation on defect-rich MgO and the smallest size for which the low temperature ($T < 250$ K) combustion was detected is Au_8. For larger sizes a distinct size dependence has been observed (figure 2(a)), with roughly two temperature regions for CO oxidation: $T < 250$ K and $T > 250$ K, which can be associated with different reaction mechanisms (see below). As expected, gold films are inert for CO oxidation. By integrating the total area in the mass spectra, the total number of CO_2 molecules formed per cluster can be plotted vs. the number of atoms per cluster (figure 2(b)). No linear dependence of the reactivity as a function of size can be observed indicating clearly

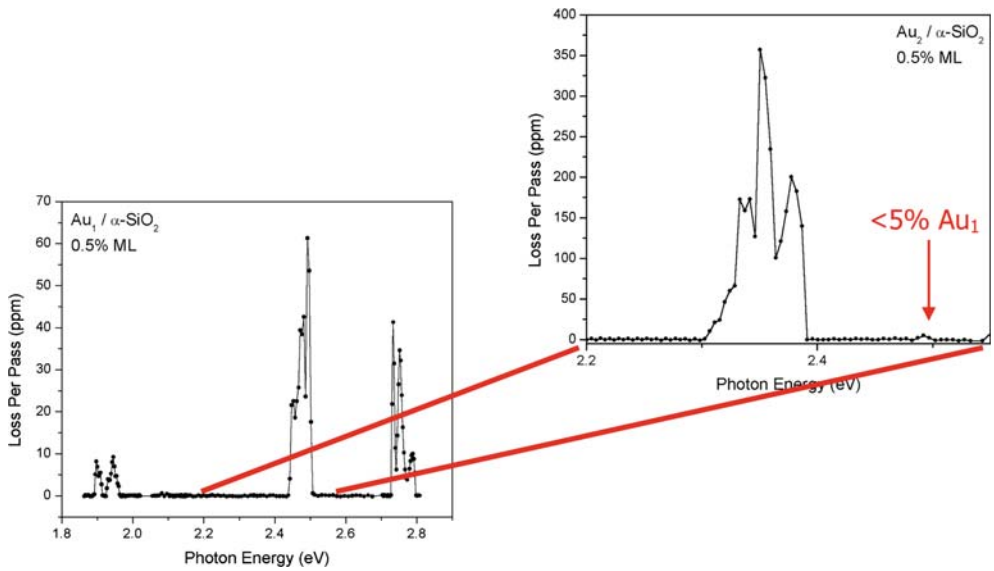

Figure 1. Shown are the measured optical responses of Au_1 and Au_2 deposited on amorphous SiO_2. Note that in the Au_1 spectrum no features of Au_2 are observed, indicating that coalescence can be excluded. In the spectrum of Au_2 a very weak optical response is observed just below 2.5 eV, which might originate from gold atoms. If this feature is attributed to single Au atoms then the fragmentation of Au_2 upon deposition is less than 5%. Note that in this energy range also a small feature of Au_2 is predicted by *ab-initio* calculation. Both spectra have been measured by cavity ring-down spectroscopy.

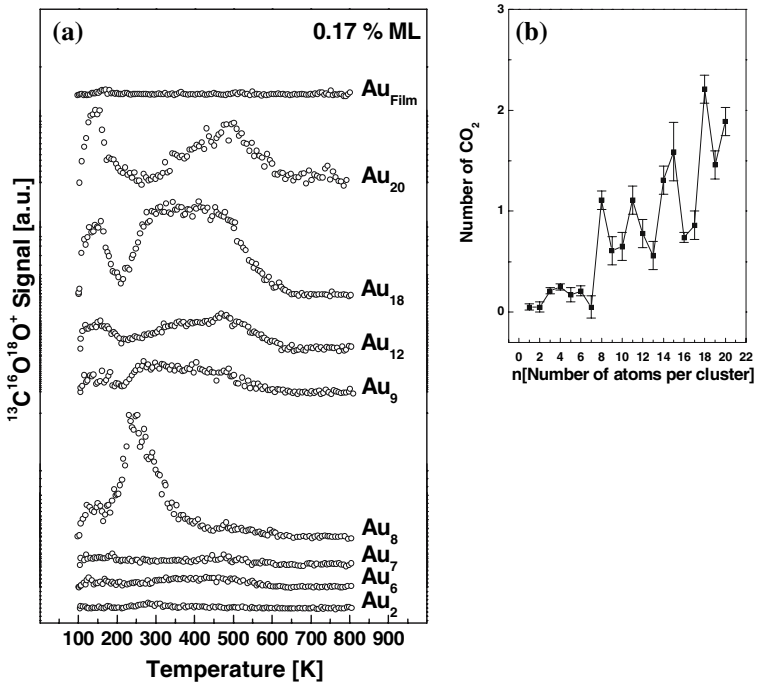

Figure 2. (**a**) Temperature programmed reaction experiments for the CO-oxidation on selected Au_n clusters on defect-rich MgO(100) films. The model catalysts were saturated at 90 K with ^{13}CO and $^{18}O_2$ and the isotopomer $^{13}C^{18}O^{16}O$ was detected with a mass spectrometer, as function of temperature. (**b**) The reactivities for Au_n expressed as the number of formed CO_2 per cluster.

that the number of reactive sites differs for each cluster size.

3. The reaction mechanism

Turning our attention to the reaction mechanism, for the CO oxidation reaction on gold clusters supported on MgO films, two main characteristics are notable. The TPR spectra shown in figure 3, were obtained for the CO oxidation reaction catalyzed by Au_8 clusters supported on defect-poor and defect-rich MgO films. These spectra show first that the reactivity is strongly dependent on the number of defects on the support (see below). Secondly, for reactive gold clusters (see also figure 2), two temperature ranges may be distinguished, i.e. roughly $T < 250$ K and $T > 250$ K. Concerning the two temperature ranges, two different reaction pathways may contribute to the oxidation of CO. We note here that due to the reaction conditions [18] peaks in the TPR spectra may be associated with Langmuir-Hinshelwood (LH) reaction mechanisms. Indeed, two different LH-type mechanisms were predicted by first-principles simulations of the reaction [18]. With the observed formation of CO_2 at 140 K (figure 4(a–c)), we associate a reaction where the two reactants are co-adsorbed initially on the triangular top facet of the Au_8, hence the name LHt mechanism. The distance between the carbon atom and one of the peroxo oxygens in this local minimum energy state is equal to $d(CO_1) = 3.11$ Å. Through mapping of the potential energy surface along the C–O_1 reaction coordinate, a rather low energy barrier ΔE_b (LHt) = 0.1 eV occurring at $d(CO_1) \approx 2.0$ Å was determined for the LHt oxidation channel, with the end product being a weakly adsorbed carbon dioxide molecule (~0.2 eV). The LHt low-temperature oxidation mechanism was found by these theoretical studies (with similar energetics), for reactions on the gold cluster deposited on either a defect-free MgO(100) surface, or one containing an F center (FC) defect site [18] and both are expected to be relatively insensitive to the Au_n cluster size, correlating with the experimental results (figures 2 and 3).

As shown in figure 3, the higher temperature channel is strongly enhanced for Au_8 supported on a defect-rich (compared to a defect-poor) MgO(100) support. This trend correlates with the prediction obtained from the simulations pertaining to a LH-periphery (LHp) reaction mechanism, starting with a CO molecule adsorbed on the top-facet of the Au_8 cluster and an oxygen molecule in a peroxo-like state that is bonded to the periphery of the interfacial layer of the cluster, where the distance between the C atom and the oxygen marked O_1 is $d(CO_1) = 4.49$ Å. Indeed, mapping of the potential energy surface along the C–O_1 reaction coordinate revealed for Au_8/MgO(FC) a rather broad reaction barrier $\Delta E_b(\text{LHp}) \sim 0.5$ eV at $d(CO_1) \sim 2.0$ Å (figure 4), while for the defect-free substrate a significantly higher barrier was found, $\Delta E_b(\text{LHp}) \sim 0.8$ eV; the reaction product is shown in figure 4(f) for the Au_8/MgO(FC) catalyst. This change in activation energy is at the origin of the observed change in reactivity, as for the defect-poor substrate the CO molecule desorbs prior to

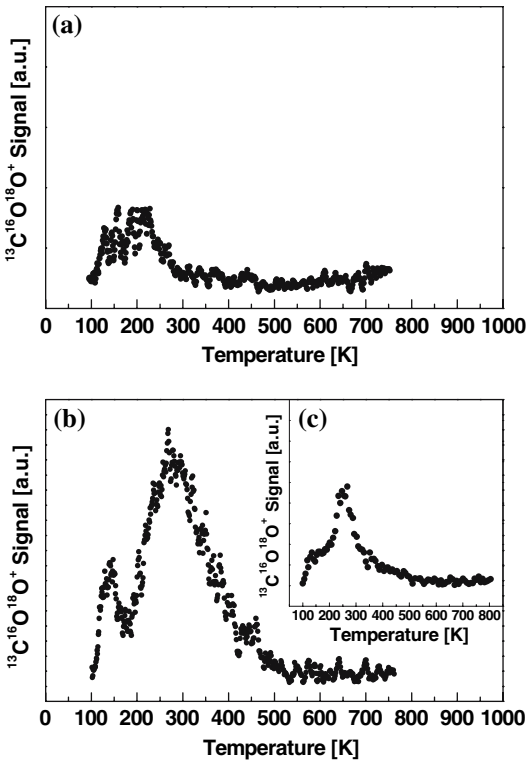

Figure 3. Temperature programmed reaction experiments for the CO-oxidation on Au_8 clusters on (**a**) defect-poor and (**b**) defect-rich MgO(100) films; inset (**c**) shows the results after producing FC on MgO(100) following the procedure of Pfnür *et al.* (see text). The model catalysts were saturated at 90 K with ^{13}CO and $^{18}O_2$ and the Isotopomer $^{13}C^{18}O^{16}O$ was detected with a mass spectrometer, as function of temperature.

reaction. The question may arise, why the two reaction channels are observed experimentally, since the low-temperature mechanism should be always dominant because its reaction rate is orders of magnitude higher. In fact, theoretical studies revealed that only one oxygen molecule adsorbs on the clusters. Thus, there exists an ensemble of Au_8 clusters with an oxygen molecule adsorbed on the periphery and another ensemble with the oxygen molecule bound to the top facet. The ratio between the number of CO_2 molecules formed at low temperature to the number formed at high temperature is in the same range as the ratio between the number of O_2 molecules which adsorb directly on the Au_8 cluster (leading to O_2 adsorbed on the top facet of Au_8) to the number of molecules which adsorb onto the cluster via reverse spill-over from the MgO substrate (leading to O_2 adsorbed at the periphery of the Au_8 cluster).

In addition to the two LH-type mechanisms, a third reaction path was found in the calculations, starting from the optimal configuration of an activated O_2 molecule adsorbed on the $Au_8/MgO(F_{5c})$ catalyst. A gas phase CO molecule brought to the vicinity of the peroxo molecule reacts spontaneously (without an energy barrier), forming a carbon dioxide molecule weakly bound to the catalyst. Therefore, this reaction (figure 4(g, h)) corresponds to an Eley-Rideal (ER) type mechanism, which can occur even at 90 K, that is during the initial dosing stage in the experiment.

4. The role of the MgO substrate

In the following, we take a closer look at the influence of surface defects on the activity of the smallest active gold cluster on MgO, i.e. Au_8. As aforementioned, the theoretically predicted strong influence of defect structures of the MgO substrate on the reactivity of the Au_8 clusters is apparent in the experiments (figure 3). An important class of point defects in MgO are oxygen vacancies, their direct characterization on the surface, however, is not straightforward. Singly charged surface oxygen vacancies (F^+-centers) have been characterized recently by electron paramagnetic resonance (EPR) measurements [48]. Neutral F-centers are not susceptible to EPR spectroscopy, but have been investigated by scanning tunneling microscopy and spectroscopy (STM and STS) [49,50]. On MgO films prepared with low deposition rates, Au_8 clusters are essentially inert. On the other hand, Au_8 clusters are found to be catalytically active on defective MgO(100) films, prepared by using high deposition rates [18]. On the latter films Au_8 clusters lead to the formation of CO_2 at 140 and 280 K. Note, that these observations are independent of the preparation procedure for defect-rich MgO films, that is, films prepared by high deposition rates show the same results as films with a high density of FC prepared after the methodology of Pfnür *et al.* [51] (see figure 3(c)). This finding suggests F-centers to play a deciding role concerning the reactivity of deposited Au_8 clusters.

The influence of F-centers on MgO(100) films on the reactivity of gold clusters was studied in more detail by FTIR, using CO that serves here, at the same time, both as reactant and as a probe molecule. These experiments were combined with extensive density-functional theory calculations. In the FTIR spectra, shown in figure 5, CO stretch frequencies at 2102 cm^{-1} and 2077/2049 cm^{-1} (Au_8 on defect-poor and defect-rich films, respectively) are observed as well as a band at 1300 cm^{-1}, which is tentatively attributed to highly activated O_2, indicating that both reactants, CO and O_2, are adsorbed molecularly at 90 K [15]. For the reactive model catalyst the disappearance of these vibrational bands coincides with the formation of CO_2 (figure 5(right)), whereas, in the case of the unreactive (figure 5(left)) model catalyst (Au_8/MgO(defect-poor)), the two reactants simply desorb from the sample, as monitored by mass spectrometry [18,19]. From theoretical studies, three energy-optimized deposited cluster configurations pertinent to the experimental conditions are obtained (figure 6). The bare adsorbed Au_8 cluster (figure 6(a)) exhibits only a slight distortion from the structure of the corresponding gas-

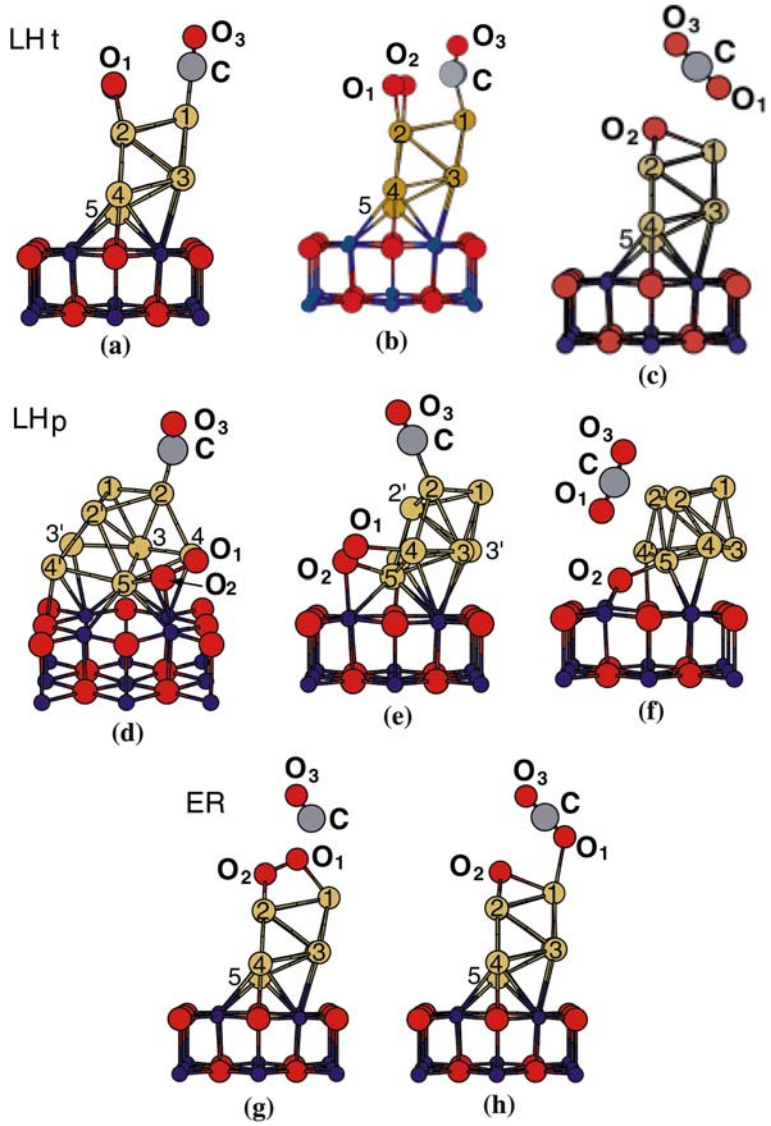

Figure 4. Reaction mechanisms of the CO oxidation on Au_8.

phase neutral cluster [19]. However, the strong influence of F-centers is reflected in the calculated binding energy of Au_8 to the defective MgO surface (3.445 eV) and to the defect-free surface (1.225 eV), respectively; for details of the calculations, see Ref. [19]. Optimal geometries with a single adsorbed CO molecule, $Au_8/O_2/CO/MgO(FC)$, and at saturation coverage of the cluster (i.e. with three adsorbed CO molecules, $Au_8/O_2/(CO)_3/MgO(FC)$), are shown in figure 6(b, c), respectively. Among the adsorbed ^{13}CO molecules at saturation coverage, only two have a significant dynamic dipole moment perpendicular to the surface, $CO^{(1)}$ and $CO^{(3)}$, consistent with the experimental observation (figure 5).

The key for understanding the influence of F-centers on the reactivity of the Au_8 cluster is the experimentally observed redshift in the CO stretch frequency by 25–50 cm^{-1} for $CO/Au_8/MgO$(defect-rich), compared to $CO/Au_8/MgO$(defect-poor). This shift indicates a change in the charge-state of the gold octamer bound to defective magnesia surface, since the absorption frequency of CO adsorbed on metal surfaces depends strongly on the population of the antibonding $2\pi^*$ orbital. Table 1 summarizes the calculated influence of excess charge ΔQ for the isolated $Au_8/O_2/^{13}CO$ complex. The calculations clearly show that the ^{13}CO stretch frequency shifts as a function of the charge-state of the complex. In detail, the shift is correlated with variations in the population of the antibonding state. For neutral complexes (ΔQ ($Au_8/O_2/^{13}CO$) = 0 in table 1) with zero spin, a vibrational frequency of 2009 cm^{-1} is obtained for the adsorbed ^{13}CO. The calculated decrease in frequency (61 cm^{-1}) in comparison to the value calculated for the free molecule is attributed to a net excess charge (0.285e^-) on the adsorbed molecule, resulting from back-donation into the $CO(2\pi^*)$ antibonding state. As expected, such donation of charge from occupied

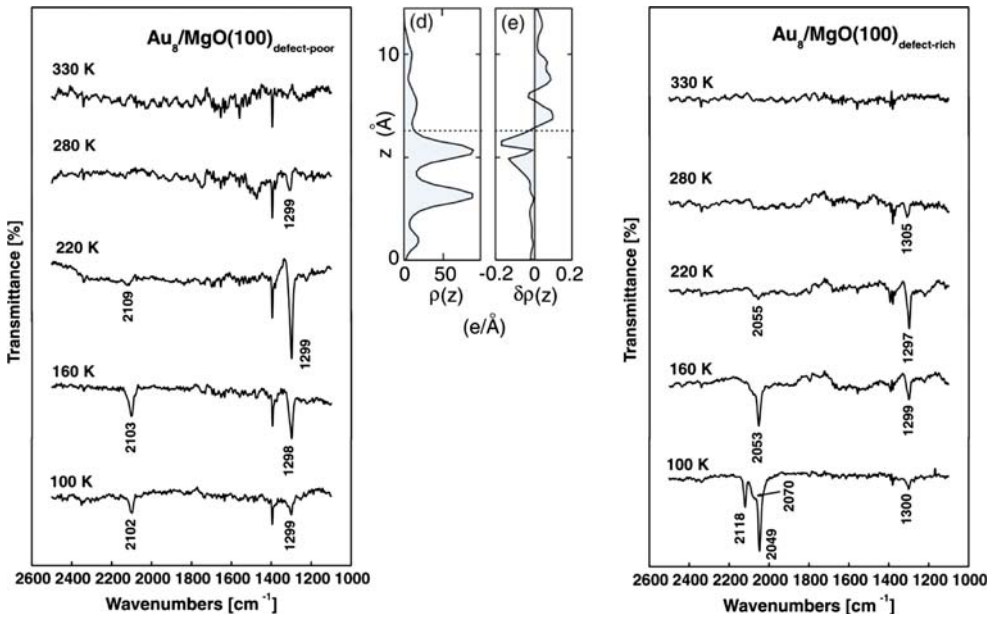

Figure 5. FTIR spectra taken at 90 K after exposing the model catalysts (left) $Au_8/MgO(100)_{defect\text{-}poor}$ and (right) $Au_8/MgO(100)_{defect\text{-}rich}$ to ^{13}CO and O_2 and annealing the sample to the indicated temperature. The frequencies between 2050 and 2100 cm^{-1} are attributed to adsorbed CO, whereas the band at 1300 cm^{-1} may originate from activated O_2 molecules. Note, the redshift of the CO-stretch by 50 cm^{-1} on defect-rich films. This shift is consistent with the predicted charging of the cluster when deposited on an F center (middle inset), where the difference of the charge densities of the isolated (Au_8, MgO(FC)) and the model system (Au_8/MgO(FC)) was calculated. The charging was estimated to be 0.5–1.0 e^-.

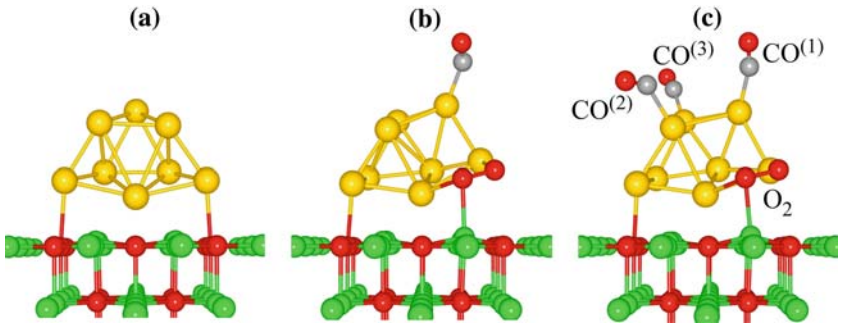

Figure 6. Optimized configurations of: (**a**) a bare gold octamer (yellow spheres), adsorbed on an F-center of an MgO (001) surface (oxygen atoms in red and magnesium in green); (**b**) a surface-supported gold octamer with an oxygen molecule, adsorbed at the interface between the cluster and the magnesia surface. Note, the significant change in the geometry of the cluster compared to the one shown in (a); (**c**) the gold octamer on the magnesia surface (MgO(FC)) with three CO molecules (carbon in gray and oxygen in red), adsorbed on the top facet of the cluster and an oxygen molecule, preadsorbed at the interface between the cluster and the magnesia surface. Note, that the molecule marked $CO^{(2)}$ lies parallel to the surface and is thus, not infrared active in the experimental configuration employed here. The C–O bond length $d(CO^{(i)})$, the charge transferred to the $CO^{(i)}$ molecule $\Delta Q^{(i)}$, and the calculated C–O vibrational frequency $\nu^{(i)}$, i = 1,2, and 3, as well as the corresponding values for the O_2 molecule, are: $d(CO^{(i)})$ [Å] = 1.151, 1.158, 1.153, $d(O_2)$ = 1.422; $\Delta Q^{(i)}$ [e] = 0.306, 0346, 0.319, $\Delta Q(O_2)$ = 1.125; $\nu^{(i)}$ [cm^{-1}] = 1993, 1896, 1979, $\nu(O_2)$ = 895.

orbitals of the metal to unoccupied states of the adsorbed molecule is even more pronounced (0.88e^-) for the more electronegative di-oxygen molecule. Upon charging the complex with up to 0.5e^-, the net excess charge on the ^{13}CO molecule is increased to 0.34e^- and it is reflected in a redshift of the CO stretch frequency (1975 cm^{-1}) by 34 cm^{-1} with respect to the neutral cluster case (2009 cm^{-1}). Concurrently, the C–O bond-length is increased (see table 1). A similar behavior is also found, when starting from the triplet state of the neutral complex. The actual degree of charge transfer can be deduced directly from *ab-initio* calculations, where the charge density of the Au_8/MgO(FC) system is compared with the isolated system (Au_8, MgO(FC)) [18,19]. The difference of the two charge density plots predicts a charge transfer of 0.5e^- into the cluster (see inset in figure 5). Comparing theory and experiment, the experimentally observed redshift in the C–O stretch for the molecule adsorbed on differently prepared MgO (defective and defect-poor) films is thus provides direct experimental evidence for the existence of high concentration of FC on our defect-rich MgO films.

Table 1
Vibrational frequencies of the $Au_8O_2{}^{13}CO$ complex (gas-phase) as function of charging

ΔQ ($Au_8O_2{}^{13}CO$)	Spin	ν (cm^{-1})	BE(O_2 + ^{13}CO) (eV)	$d(^{13}CO)$ (Å)	$\Delta Q(^{13}CO)$	$d(O_2)$ (Å)	$\Delta Q(O_2)$
0	1	2005	1.060	1.149	0.29	1.336	0.71
0.25	0.875	1987		1.150	0.32	1.344	0.75
0.5	0.75	1968		1.154	0.35	1.350	0.77
1.0	0.5	1926		1.160	0.43	1.364	0.86
0	0	2009	0.753	1.148	0.28	1.378	0.88
0.25	0	1990		1.150	0.31	1.381	0.89
0.5	0	1975		1.153	0.34	1.385	0.92
1.0	0	1920		1.158	0.41	1.398	1.00

Results for free ($Au_8O_2{}^{13}CO$) complexes as a function of excess electron charge ΔQ. The results are shown for various values of the spin; for the neutral cluster, we show triplet (S = 1) and singlet (S = 0) states. The displayed quantities are: ν – the CO stretch frequency; BE(O_2 + ^{13}CO) – the CO binding energy to the gold cluster with a preadsorbed oxygen molecule; the bond distances, $d(^{13}CO)$, $d(O_2)$, and excess electronic charges, $\Delta Q(^{13}CO)$, $\Delta Q(O_2)$, of the two adsorbed reactants CO and O_2. We remark for reference, that the calculated vibrational frequency of gas-phase ^{13}CO is 2070 cm^{-1} ,which is 25 cm^{-1} smaller than the experimental value of ν (^{13}CO) = 2095 cm^{-1}.

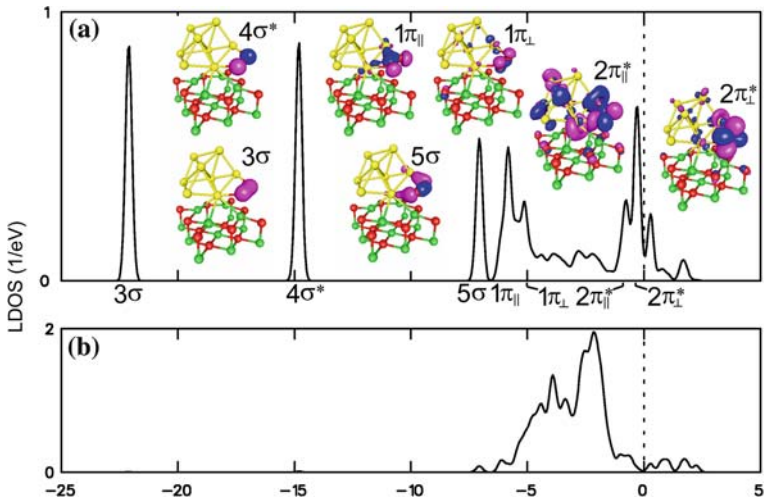

Figure 7. Local density of the electronic states (LDOS) of $Au_8/O_2/MgO(100)FC$. For these studies the O_2 molecule was adsorbed on the periphery and no CO molecules were co-adsorbed in order to separate the interaction of O_2 with the cluster from coupling effects between the reactants. The prominent peaks of the oxygen LDOS are labeled following the conventional nomenclature for the molecular orbitals of the gas-phase O_2 molecule, with $\perp$ and $||$ meaning perpendicular and parallel to the MgO surface, respectively. The Fermi energy is at 0 eV.

The consequences of the charge transfer from the oxygen vacancy into the deposited Au_8 cluster, for the binding and activation of the two reactants can be outlined by analyzing the local density of electronic states (LDOS), projected on the oxygen molecule, adsorbed at the periphery site of $Au_8/MgO(FC)$ (figure 7(a)). All the prominent peaks can be unambiguously assigned to orbitals of (free) molecular oxygen origins. In addition, these states overlap with the entire d-band of the Au_8 cluster (figure 7(b)) in the range of $-7\ eV \le E \le E_F$, where E_F is the Fermi energy. Bonding of the oxygen molecule to the gold octamer involves mainly hybridization of the 5σ, $1\pi_{||}$, and $1\pi_{\perp}$ oxygen states with the gold d-band. Most importantly, the full spin-manifold of the antibonding $2\pi^*$ states of O_2 is located below E_F, resulting in strong activation of the O_2 molecule through occupation of the antibonding orbitals. This leads to weakening of the O–O bond that is reflected in a significant increase of its length (1.43 Å), compared to that of the free molecule (1.25 Å), and the molecule is adsorbed in a peroxo-like state [19]. We observe that O_2 binding to the cluster is stronger in the presence of the F-center (0.47 and 0.33 eV for the spin 0 and spin 1 states, respectively), in comparison to the case without F-centers (0.33 and 0.30 eV for the spin 0 and spin 1 states, respectively). The bonding of CO to the $Au_8/O_2/MgO(FC)$ complex can be understood by analyzing the correlation diagram, shown in figure 8. It depicts LDOS for the two reactants, CO (figure 8(left)) and the $Au_8/O_2/MgO(FC)$ complex (figure 8(right)), as well as for the product complex $Au_8/O_2/CO/MgO(FC)$, with the CO adsorbed on the deposited cluster (figure 8(middle)). As expected, the 3σ and the non-bonding 4σ molecular orbitals of the isolated CO are not

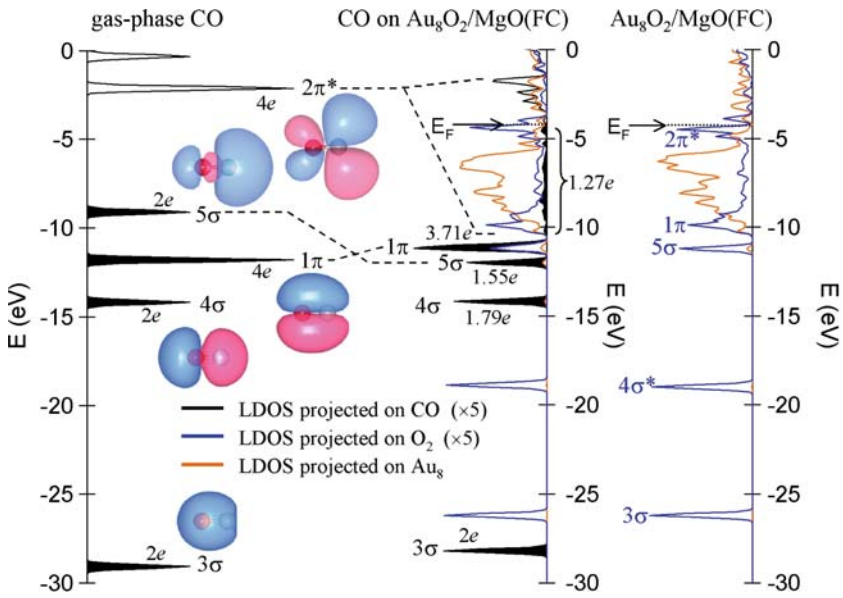

Figure 8. Local density of states (LDOS) correlation diagram of free CO (left) and $Au_8/O_2/MgO(FC)$ (right), resulting upon adsorption of the CO molecule in the complex on $Au_8/O_2/CO/MgO(FC)$ (middle). The color assignments in the LDOS diagrams are given in the figure. The electron populations of the various levels are given as 2e, 4e, etc., and iso-surface images of the orbitals of the free CO molecules are also shown (left). Dashed lines indicate orbital shifts and redistribution, caused by the adsorption of the CO molecule.

involved in the bonding to the cluster complex as their energies are not changed upon adsorption. On the other hand, the non-bonding 5σ orbital is stabilized by the interaction (by about 3 eV) and thus it contributes to the chemisorption of carbon monoxide to the surface-supported complex through hybridization with the metal-cluster orbitals. The 1π level is slightly pushed upward in energy (<1 eV). The largest contribution to the bonding of CO to the complex occurs via hybridization of the antibonding $2\pi^*$ levels of CO and the occupied frontier electronic states of the cluster complex. The $2\pi^*$ orbitals are pushed below the Fermi level, partially populating this molecular state, i.e. the so-called backdonation [52]. All these features are also present in the correlation diagram of the cluster complex bound to the defect-free MgO surface, where backdonation, however, is less pronounced.

5. Electronic size effects

Understanding the size-dependent electronic structure of the $Au_n/MgO(FC)$ model catalysts is fundamental for elucidation of their atom-by-atom controlled reactivity. As discussed above, bonding and activation of O_2 at the periphery site of the $Au_8/MgO(FC)$ model catalyst, is enabled by resonances formed between the cluster's electronic states and the $2\pi^*$ molecular states of oxygen. A drastically different scenario is found for the interaction of O_2 with a smaller gold cluster, $Au_4/MgO(FC)$, where molecular oxygen adsorbs in an "on-top" configuration, with one of the oxygen atoms binding to a single gold atom [53]. This system exhibits rather weak binding of the molecule to the metal cluster (0.18 eV) and an almost unperturbed O–O bond length. The weak binding can be attributed to the narrower d-band of the adsorbed Au_4 cluster, compared to that of Au_8, with a consequent lack of overlap between the states at the bottom of the d-band of the gold cluster and the molecular oxygen states, with energies $E < -5$ eV. Moreover, the antibonding $2\pi_\perp^*$ and $2\pi_{||}^*$ orbitals of the adsorbed oxygen molecule are located above E_F, which results in no activation of the molecule by the adsorbed Au_4 cluster; for further details see Ref. [53].

6. Structural dynamical fluxionality

The capability of small clusters to exhibit several structural forms (isomers) of comparable energies, and to interconvert between such isomers at finite temperature, is one of the hallmarks of cluster science. This unique structural variability may influence the chemical reactivity of nano-catalytic systems in two main ways. First, at finite temperature, the model catalyst will form an equilibrium ensemble of coexisting structural configurations, with various isomers, exhibiting different chemical reactivities. Second, and most importantly, is the structural dynamic fluxionality of clusters in the course of reactions, that expresses itself in the ability of a given structural isomer to dynamically adapt its structure, such as to allow the reaction to evolve on the most favorable free-energy path. Such fluxional propensity is illustrated in figure 6(a–c), comparing the adsorbed bare-cluster geometry with those of the gold cluster, with adsorbed reactant molecules on it. The structural fluxionality is essential for the reaction to

occur, since it was found that constraining the cluster to maintain its original geometry prevents the adsorption and activation of O_2 [53].

7. Tuning of the catalytic activity of Au nanoclusters via support design

One of the goals of research in nanocatalysis is the control and tuning of catalytic activity. Most recently tuning of the catalytic activity of gold nanoclusters through the design of the underlying support has been explored [54]. It was shown that gold clusters adsorbed on a very thin (two layers) defect-free MgO film which is itself supported on Mo(100) [55], may serve as model catalysts for the low-barrier oxidation of CO. The origin of the emergent activity of the nanoclusters is a dimensionality crossover of the adsorbed gold clusters, from inactive three-dimensional (3D) optimal structures on thick MgO films, to catalytically active 2D ones for sufficiently thin MgO films (less then 1 nm in thickness) supported on Mo(100). The increased gold wetting propensity on the MgO/Mo(100) surface originates from electrostatic interaction between the underlying metal and metal-induced excess electronic charge accumulated at the cluster interface with the metal-oxide film [56]. The excess interfacial charge is predicted to activate O_2 molecules adsorbed at the interfacial periphery of the 2D gold island with the MgO/Mo(100) surface. This activation, which weakens greatly the O–O bond, lowers rather remarkably the barrier for reaction of the activated molecule with CO and the subsequent emission of CO_2.

While details of the calculations can be found elsewhere [2,54,56] we take this opportunity to give some pertinent detail. The first-principles calculations used in studies are based on a density functional theory approach [57–59] with exchange and correlation energy corrections included through a generalized gradient approximation (GGA) [60]. A plane wave basis is used with a cutoff kinetic energy of 30 Ry, and ultrasoft pseudopotentials (scalar relativistic for Au) [61] are employed with Γ-point sampling of the Brillouin zone. In structural relaxations corresponding to minimization of the total energy, convergence is achieved when the forces on the atoms are less than 0.001 eV/Å.

In modeling the metal-supported MgO films a four-layer Mo(100) slab (lattice constant of 3.15 Å) of thickness 4.64 Å was used, since it has been found to reproduce (in its middle) the bulk electronic properties of Mo [62]. The planar Au_{20} clusters was adsorbed on a MgO/Mo(100) with 5×6 unit cells of the Mo(100) surface; for the 3D tetrahedral cluster the dimensions of the MgO surface (without the metal support) were the same, and the bottom layer of the metal oxide was held fixed. In all calculations, the periodically replicated slabs were separated [in the (100) direction] by a vacuum region of 20 Å. In structural optimizations all the atoms of the adsorbed gold clusters, the MgO thin film, and the first two layers of the Mo substrate were allowed to relax. In calculation involving the tetrahedral gold structure the MgO(100) crystalline surface was modeled by a two-layer MgO(100) slab which is sufficiently thick to both reproduce the properties of the bare MgO surface [63], and to obtain converged results (with respect to the number of MgO layers) for the energetics of adsorbed Au clusters [30].

The gas-phase optimal 3D tetrahedral Au_{20} cluster [64] was found to maintains its structure on the MgO(100) surface, with a 1.2 eV advantage over the planar structure [56] (figure 9). However, this cluster adsorbs O_2 only weakly (0.34 eV on the top apex atom of the pyramid with d(O–O) = 1.28 Å remaining close to the gas phase value), and no binding was found at peripheral sites of the gold/MgO interface; when CO is preadsorbed at the top apex Au atom (0.7 eV) no coadsorption of O_2 occurs.

In light of the above inactivity of the 3D structure we focused our investigations on Au_{20} adsorbed on a

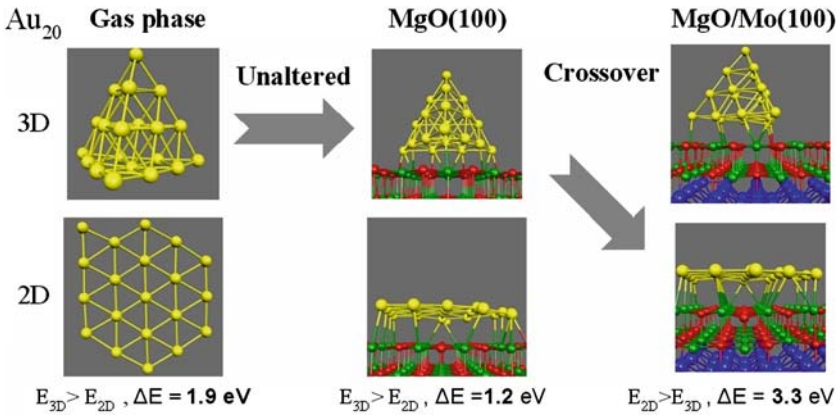

Figure 9. The dimensionality crossover of Au_{20}, from a 3D stable structure in the gas phase (left) and when adsorbed on MgO(100), to a 2D island when adsorbed on the surface of a two-layer thin MgO film supported on Mo(100), MgO/Mo(100). The absolute values of the adsorption energies are given; e.g., $E_{2D} > E_{3D}$ indicates a more stable 2D structure.

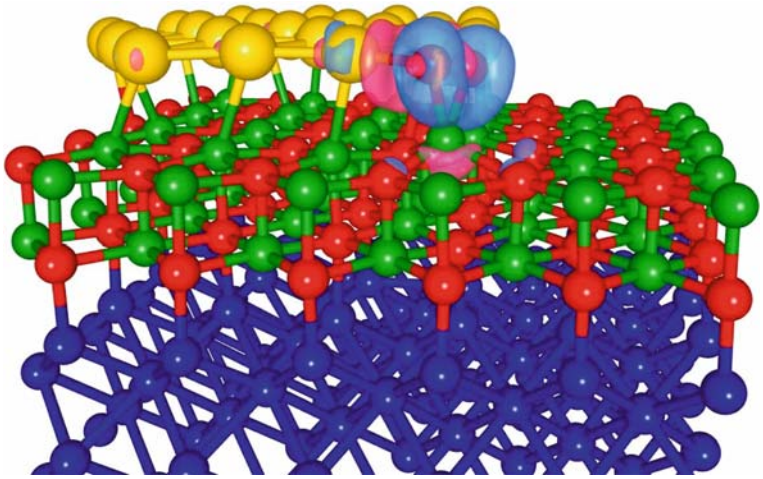

Figure 10. Two dimensional Au_{20} island (yellow on line) adsorbs on a two-layer MgO film (O atoms in red and Mg in green) supported on Mo (100) (blue on line), with a coadsorbed O_2 molecule. Superimposed we show an isosurface of the excess electronic charge (light blue on line) illustrating activation of the adsorbed molecule through population of the antibonding $2\pi^*$ orbital.

two-layer MgO/Mo(100). Here the planar isomer is more stable then the 3D one by 3.3 eV (see figure 9), with the enhanced stability resulting from penetration of metal states through the thin MO film and charge accumulation at the cluster/MgO interface (up to 1e for Au_{20}) [56]. Furthermore, in this configuration the O_2 adsorbs relatively strongly (1.35 eV) at the cluster periphery (figure 10), and the process is accompanied by transfer of electronic charge (about 1.3e) into the antibonding $2\pi^*$ orbital leading to activation of the O–O bond of the adsorbed molecule into a peroxo state with d(O–O) = 1.52 Å and no spin polarization.

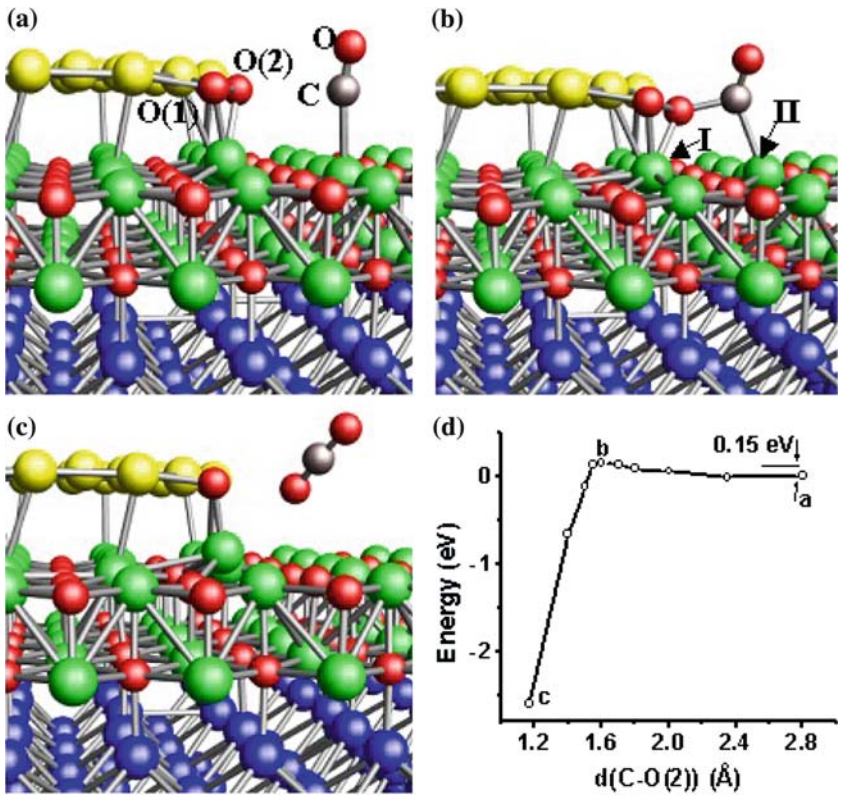

Figure 11. (a–c) Configurations of the two dimensional Au_{20} island shown in figure 1 (the color scheme is the same as in figure 1) with coadsorbed O_2 (the atoms marked O(1) and O(2), and CO (C atom in gray online). (**a**) the initial optimized configuration; d(O(1)–O(2)) = 1.52 Å, d(C–O(2)) = 2.85 Å. (**b**) The transition state (the nearest neighbor Mg atoms are marked as I and II. Distances are: d(O(1)–O(2)) = 1.55 Å, d(C–O(2)) = 1.60 Å, d(C–O) = 1.18 Å, d(C–Mg(II)) = 2.30 Å. (**c**) a configuration illustrating formation and desorption of CO_2. (**d**) The total energy profile along the C–O(2) reaction coordinate, with the zero of the energy scale taken for configuration (a). The sharp drop past the barrier top corresponds to CO_2 formation.

Two mechanisms for the reaction of CO with the activated oxygen molecule were probed. Various CO coadsorption sites were probed. First, adsorption to the gold cluster was examined yielding relaxed adsorption configurations with CO binding energies ranging from 0.8 eV (CO binding to a peripheral Au atom that is nearest-neighbor to the Au atom bonded to the O_2), down to a vanishingly small binding for a non-periphery nearest-neighbor Au atom on the flat gold island. However, calculation of the barrier [54] for reaction between the reactants (with CO at the peripheral site) yielded a high value of close to 1.0 eV.

We have tested also several CO coadsorption sites located on the MgO surface in the vicinity of the adsorbed O_2. The adsorption geometry shown in figure 11(a) is characterized by a CO binding energy of 0.4 eV. Starting from this coadsorption configuration the LH reaction barrier leading to formation of CO_2 was calculated to be 0.15 eV; the transition state is shown in figure 11(b), CO_2 formation in figure 11(c), and the energy profile along the reaction coordinate is displayed in figure 11(d). The product molecule desorbs readily in the course of the reaction (the binding energy of CO_2 to a Mg site on the MgO(100) surface is merely 0.14 eV). Alternatively, several reaction trajectories that follow the ER mechanism were probed. Some of these trajectories yielded formation of CO_2 with a small (0.2 eV) or vanishngly small barriers, depending on the angle of approach.

These results serve to illustrate one of the methodologies that may be employed in attempting to control the reactivity of adsorbed gold nanostructures through manipulations of the supporting substrate. Such an approach may be coupled with other developments for controlling the interfacial charge (and consequently the chemical reactivity) in nanocatalytic systems, for example, through the use of applied fields.

8. The effect of water

As mentioned in the introduction, for certain supports, moisture is able to increase the activity of gold nanocatalysts by about two orders of magnitude [24] Thus, the influence of water on the chemical activity of gold clusters was recently investigated with the use of quantum mechanical *ab-initio* calculations for Au_8 adsorbed on a defect-free MgO(100) surface [65], i.e. a system that does not exhibit charging effects and is inert for CO oxidation (see above).

The influence of water (co-)adsorption manifests itself in the calculated change of the oxygen binding energies. For the gold octamer, bound to a defect-free MgO(100) surface, two spatial regions for oxygen adsorption may be identified in the calculations: (i) the top facet of the cluster, where O_2 adsorbs weakly (adsorption energies up to 0.1eV), in agreement with [18,27,30] and (ii) peripheral sites (at the Au_8/MgO interface), where O_2 adsorbs with energies between 0.3 and 0.8 eV (Table 2), with the O–O bond extended to 1.37–1.49 Å. Water adsorbs (relative weak) on free and supported Au clusters (table 2), with adsorption energies that vary from 0.2 to 0.6 eV, and without apparent correlation between the adsorption strength and the coordination of the adsorption site. Interestingly, it was found that an adsorbed H_2O is an "attractor" for molecular O_2 and in the presence of an adsorbed water molecule O_2 preferentially adsorbs at a neighboring site. Moreover, it may bind even at sites where the adsorption of O_2 (without coadsorbed H_2O) is energetically unfavorable.

Table 2
Energies (in eV) for the adsorption and coadsorption of O_2 and H_2O on free Au_8 and on a gold octamer supported on MgO(100), that is Au_8/MgO

	O_2	H_2O	H_2O–O_2
Au_8	Unbound	~0.3	0.4–0.9
Au_8/MgO-T	≤0.1	0.2–0.3	0.5–1.2
Au_8/MgO-P	0.3–0.8	0.4–0.6	1.3–2.1

In the case of the Au_8/MgO system, results are given for both the adsorption on the top-facet of the gold cluster (-T) and at the peripheral interface of the cluster with the substrate (-P).

In some cases of H_2O and O_2 coadsorbed on the top facet of Au_8/MgO, the proton shared by the H_2O and O_2 molecules may actually be considered as transferred to the O_2 species and an OH and a hydroperoxyl-like (HO_2) group are formed; for details see [65]. The distance between the O atoms sharing the proton takes a value of about 2.49 Å, while the O–O hydroperoxyl bond length reaches a value of about 1.48 Å (that is 21% larger than in a free molecule), reflecting a very high degree of bond activation. A charge analysis shows, that an amount of approximately 0.31e is transferred from the Au_8/MgO system to the coadsorbed species. These results suggest that the coadsorption of H_2O and O_2 stabilizes partially charged highly activated states of the adsorbed oxygen molecule. No such bond-activation is found for the adsorption of O_2 on the top-facet of the supported gold octamer without water coadsorption. MgO surfaces are hydrophilic and H_2O molecules adsorb with energies of about 0.4 eV. In the vicinity of the peripheral interfacial sites of the Au cluster the calculations showed, that the adsorption energy of H_2O increases by 0.1–0.2 eV (depending on the particular site and adsorption configuration); thus, the gold cluster acts as an attractor for adsorbed water (reverse spillover). Hence, at the interface between the Au cluster and the MgO surface, peripheral sites show a high propensity to bind both H_2O and O_2 (Table 2). The markedly larger binding energies of the coadsorbed complex (compared to the individual adsorbates) reflect a synergetic effect, expressed through the occurrence of the aforementioned proton sharing and proton transfer processes.

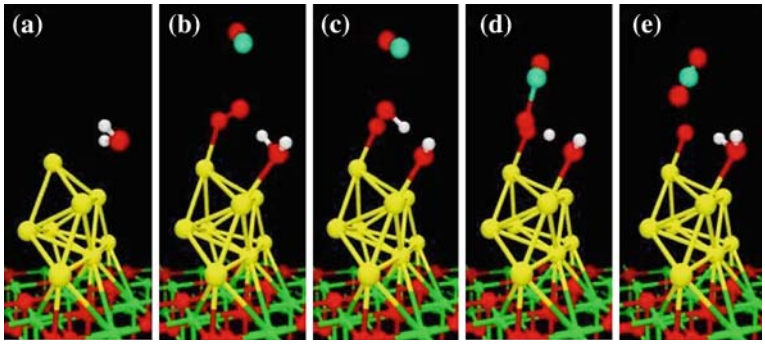

Figure 12. Relaxed atomic configurations, displaying several stages in the simulation of the coadsorption of H_2O and O_2 on the top-facet of an Au_8 cluster supported on MgO(100), and the subsequent reaction with gaseous CO to form CO_2. (**a**) The approach of an H_2O molecule to the cluster. (**b**) Coadsorbed H_2O (right) and O_2 (left) with an approaching CO. Note, the preferential orientation of the H_2O and partial proton-sharing. (**c**) CO-induced proton transfer, resulting in formation of a hydroperoxyl-like group (left) and a hydroxyl (right). (**d**) Transition state configuration with the CO binding to the activated species. The proton is about midway between one of the oxygens of the transition-state complex (left) and the hydroxyl (right). (**e**) The proton shuttles back to reform an adsorbed H_2O, and the CO_2 product desorbs from the surface, leaving an adsorbed oxygen atom that reacts in the next step with a CO molecule, to yield a second CO_2. Yellow, red, white and magenta colored spheres correspond to Au, O, H and carbon atoms, respectively.

To address the reactivity of O_2 coadsorbed with H_2O on the top facet of the adsorbed gold cluster, a sequence of adsorption and reaction steps that result in the catalytic oxidation of CO, is displayed in figure 12. Starting from the bare Au_8/MgO system, an H_2O molecule adsorbs first (figure 12(a)). Subsequently, an O_2 molecule is coadsorbed and the system is exposed to incident CO (see the proton-sharing configuration in figure 12(b)). In figure 12(c), a proton transfer process, induced by the incoming gaseous CO molecule is shown, leading to formation of a hydroperoxyl-like complex. Upon reaction of the CO molecule with the complex, the proton shuttles back towards the hydroxyl group (figure 9(d)), with the process culminating in the desorption of a CO_2 molecule and reformation of an adsorbed H_2O molecule that is preferentially oriented with respect to the remaining adsorbed oxygen atom figure 12(e)). The above ER-like reaction mechanism involves relatively low barriers. It was found that the formation of the transition state (figure 12(d)) entails a readily accessible energy barrier of $\sim$0.5 eV. An added CO molecule reacts readily (a barrier of 0.1 eV) with the single adsorbed oxygen atom, and the (barrierless) desorption of the CO_2 product closes the catalytic cycle. For a peripherally adsorbed O_2 reacting with a CO molecule adsorbed in its vicinity, a Langmuir-Hinshelwood reaction barrier of 0.4 eV was found (with or without a neighboring coadsorbed H_2O molecule). The barrier for desorption of the CO_2 product is 0.6 eV under dry conditions and 0.3 eV with coadsorbed H_2O.

9. Summary

Focusing on size-selected gold clusters consisting of up to 20 atoms, that is, in the size regime where properties can not be obtained from those of the bulk material through scaling considerations, we summarized in this article the current state of understanding pertaining to various factors that control the reactivity and catalytic activity of such nanostructures, using the CO oxidation reaction catalyzed by the gold nanoclusters adsorbed on MgO as a paradigm. These factors include the role of the metal-oxide support and its defects, the charge state of the cluster, structural fluxionality of the clusters, electronic size effects, the effect of an underlying metal support on the dimensionality, charging and chemical reactivity of gold nanoclusters adsorbed on the metal-supported ultra-thin metal-oxide films, and the promotional effect of water. We have shown that through joined experimental and first-principles quantum mechanical calculations and simulations, a detailed picture of the reaction mechanisms in nanocatalysis, and of methods for controlling and tuning the catalytic activity, emerge.

Acknowledgments

The research of UL, BY and CZ was supported by the US Air Force Office for Scientific Research (AFOSR) and the US Department of Energy (DOE). The research of UH and MA was supported by the German Research Council (DFG), the European Community through the GSOMEN project (Technical University of Munich). Computations were performed at the DOE National Energy Research Supercomputing Center (NERSC) at Lawrence Berkeley Laboratories, and at the Georgia Tech Center for Computational Materials Science.

References

[1] U. Landman, Proc. Natl. Acad. Sci. USA 102 (2005) 6671.
[2] U. Heiz and U. Landman, *Nanocatalysis* (Springer, New York, 2006).

[3] B. Hammer and J.K. Norskov, Nature 376 (1995) 238.
[4] S.A.C. Carabineiro and D.T. Thompson, in Ref. 2, Chap. 6, p. 375.
[5] N. Saliba, D.H. Parker and B.E. Koel, Surf. Sci. 410 (1998) 270.
[6] M. Haruta, Cattech 6 (2002) 102.
[7] D.Y. Cha and G. Parravan, J. Catal. 18 (1970) 200.
[8] G.C. Bond, P.A. Sermon, G. Webb, D.A. Buchanan, P.B. Wells, J. Chem. Soc. Chem. Commun. (1973) 444.
[9] M. Haruta, N. Yamada, T. Kobayashi and S. Iijima, J. Catal. 115 (1989) 301.
[10] M. Haruta, Gold Bull. 37 (2004) 27.
[11] B. Nkosi, M.D. Adams, N.J. Coville and G.J. Hutchings, J. Catal. 128 (1991) 378.
[12] B. Nkosi, N.J. Coville, G.J. Hutchings, M.D. Adams, J. Friedl and F.E. Wagner, J. Catal. 128 (1991) 366.
[13] C.T. Campbell, Science 306 (2004) 234.
[14] M.S. Chen and D.W. Goodman, Science 306 (2004) 252.
[15] G.C. Bond and D.T. Thompson, Gold Bull. 33 (2000) 41.
[16] V.A. Bondzie, S.C. Parker and C.T. Campbell, Catal. Lett. 63 (1999) 143.
[17] V.A. Bondzie, S.C. Parker and C.T. Campbell, J. Vac. Sci. Technol. A 17 (1999) 1717.
[18] A. Sanchez, S. Abbet, U. Heiz, W.D. Schneider, H. Häkkinen, R.N. Barnett and U. Landman, J. Phys. Chem. A 103 (1999) 9573.
[19] B. Yoon, H. Häkkinen, U. Landman, A.S. Worz, J.M. Antonietti, S. Abbet, K. Judai and U. Heiz, Science 307 (2005) 403.
[20] L.M. Molina and B. Hammer, Appl. Catal. A 291 (2005) 21.
[21] O. Meerson, G. Sitja and C.R. Henry, Eur. Phys. J. D 34 (2005) 119.
[22] M. Haruta, S. Tsubota, T. Kobayashi, H. Kageyama, M.J. Genet and B. Delmon, J. Catal. 144 (1993) 175.
[23] M. Date and M. Haruta, J. Catal. 201 (2001) 221.
[24] M. Date, M. Okumura, S. Tsubota and M. Haruta, Angew. Chem. Int. Ed. 43 (2004) 2129.
[25] M. Valden , X. Lai and D.W. Goodman, Science 281 (1998) 1647. See also T.V. Choudhary and D.W. Goodman, Appl. Catal. A 291 (2005) 32, and a recent review by M.S. Chen and D.W. Goodman, Accounts Chem. Res. 39 (2006) 739. .
[26] B. Yoon, H. Häkkinen and U. Landman, J. Phys. Chem. A 107 (2003) 4066.
[27] N. Lopez and J.K. Norskov, J. Am. Chem. Soc. 124 (2002) 11262.
[28] G. Mills, M.S. Gordon and H. Metiu, Chem. Phys. Lett. 359 (2002) 493.
[29] L.M. Molina and B. Hammer, Phys. Rev. Lett. 90 (2003) 206102.
[30] L.M. Molina and B. Hammer, Phys. Rev. B 69 (2004) 155424.
[31] R. Meyer, C. Lemire, S. Shaikhutdinov and H.J. Freund, Gold Bull. 37 (2004) 72.
[32] C. Lemire, R. Meyer, S. Shaikhutdinov and H.J. Freund, Angew. Chem. Int. Ed. 43 (2004) 118.
[33] C. Lemire, R. Meyer, S.K. Shaikhutdinov and H.J. Freund, Surf. Sci. 552 (2004) 27.
[34] W.A. deHeer, Rev. Mod. Phys. 65 (1993) 611.
[35] T.G. Dietz, M.A. Duncan, D.E. Powers and R.E. Smalley, J. Chem. Phys. 74 (1981) 6511.
[36] U. Heiz, F. Vanolli, L. Trento and W.D. Schneider, Rev. Sci. Instrum. 68 (1997) 1986.
[37] U. Heiz and W.D. Schneider, Crit. Rev. Solid State Mater. Sci. 26 (2001) 25.
[38] C.L. Cleveland and U. Landman, Science 257 (1992) 355.
[39] H.-P. Cheng and U. Landman, Science 260 (1993) 1304.
[40] H-.P. Cheng and U. Landman, J. Phys. Chem. 98 (1994) 3527.
[41] M. Moseler, H. Häkkinen and U. Landman, Phys. Rev. Lett. 89 (2002) 033401.
[42] K. Bromann, H. Brune, C. Felix, W. Harbich, R. Monot, J. Buttet and K. Kern, Surf. Sci. 377 (1997) 1051.
[43] X. Tong, L. Benz, P. Kemper, H. Metiu, M.T. Bowers and S.K. Buratto, J. Am. Chem. Soc. 127 (2005) 13516.
[44] S. Fedrigo, W. Harbich and J. Buttet, Phys. Rev. B 58 (1998) 7428.
[45] K. Judai, S. Abbet, A.S. Wörz, U. Heiz and C.R. Henry, J. Am. Chem. Soc. 126 (2004) 2732.
[46] J.M. Antonietti, M. Michalski, U. Heiz, H. Jones, K.H. Lim, N. Rösch, A. Del Vitto and G. Pacchioni, Phys. Rev. Lett. 94 (2005) 213402.
[47] C. Di Valentin, A. Del Vitto, G. Pacchioni, S. Abbet, A.S. Wörz K. Judai and U. Heiz, J. Phys. Chem. B 106 (2002) 11961.
[48] M. Sterrer, E. Fischbach, T. Risse and H.J. Freund, Phys. Rev. Lett. 94 (2005) 186101.
[49] S. Schintke and W.D. Schneider, J. Phys. Condens. Matter 16 (2004) R49.
[50] M. Sterrer, M. Heyde, M. Novicki, N. Nilius, T. Risse, H.P. Rust, G. Pacchioni and H.J. Freund, J. Phys. Chem. B 110 (2006) 46.
[51] D. Peterka, C. Tegenkamp, K.M. Schröder, W. Ernst and H. Pfnur, Surf. Sci. 431 (1999) 146.
[52] G. Blyholder, J. Phys. Chem. 68 (1964) 2772.
[53] H. Häkkinen, W. Abbet, A. Sanchez, U. Heiz and U. Landman, Angew. Chem. Int. Ed. 42 (2003) 1297.
[54] C. Zhang , B. Yoon and U. Landman, J. Am. Chem. Soc. 129 (2007) 2228.
[55] This scheme is commonly employed in experimental studies of Au nanstructures adsorbed on MgO films; see M.-C. Wu, J.S. Corncillc, C.A. Estrada, J.W. He and D.W. Goodman, Chem. Phys. Lett. 182 (1991) 472, and refs. 2 and 18. .
[56] D. Ricci, A. Bongiorno, G. Pacchioni and U. Landman, Phys. Rev. Lett. 97 (2006) 36106.
[57] G. Kresse and J. Hafner, Phys. Rev. B 47 (1993) R558.
[58] G. Kresse and J. Furthmuller, Phys. Rev. B 54 (1996) 11169.
[59] R.N. Barnett and U. Landman, Phys. Rev. B 48 (1993) 2081.
[60] J.P. Perdew, J.A. Chevary, S.H. Vosko, K.A. Jackson, M.R. Pederson, D.J. Singh and C. Fiolhais, Phys. Rev. B 46 (1992) 6671.
[61] D. Vanderbilt, Phys. Rev. B 41 (1990) 7892.
[62] L. Giordano, M. Baistrocchi and G. Pacchioni, Phys. Rev. B 72 (2005) 115403.
[63] L. Giordano, J. Goniakowski and G. Pacchioni, Phys. Rev. B 67 (2003) 045410.
[64] J. Li, X. Li, J. H.-Zhai and L.-S. Wang, Science 299 (2003) 864; X. P. Xing, B. Yoon, U. Landman and J.H. Parks, Phys. Rev. B 74 (2006) 165423; B. Yoon, P. Koskinen, B. Huber, O. Kostko, B. Von Issendorff, H. Häkkinen, M. Moseler and U. Landman, Chem. Phys. Chem. 8 (2007) 157.
[65] A. Bongiorno and U. Landman, Phys. Rev. Lett. 95 (2005) 106102.